

# Influence of the circumglobal wave-train on European summer precipitation

Sajjad Saeed · Nicole Van Lipzig · Wolfgang A. Müller · Fahad Saeed · Davide Zanchettin

Received: 18 March 2013/Accepted: 4 July 2013/Published online: 11 August 2013  
© Springer-Verlag Berlin Heidelberg 2013

**Abstract** We investigate European summer (July–August) precipitation variability and its global teleconnections using the NCEP/NCAR reanalysis data (1950–2010) and a historical Coupled Model Intercomparison Project climate simulation (1901–2005) carried out using the ECHAM6/MPIOM climate model. A wavelike pattern is found in the upper tropospheric levels (200 hPa) similar to the summer circumglobal wave train (CGT) extending from the North Pacific to the Eurasian region. The positive phase of the CGT is associated with upper level anomalous low (high) pressure over western (eastern) Europe. It is further associated with a dipole-like precipitation pattern over Europe entailing significantly enhanced (reduced) precipitation over the western (eastern) region. The anomalous circulation features and associated summer precipitation pattern over Europe inverts for the negative CGT phase. Accordingly, the global teleconnection pattern of a precipitation index summarizing summer precipitation over Western Europe entails an upper level signature which consists of a CGT-like wave pattern extending from the North Pacific to Eurasia. The imprint of the CGT on European summer precipitation is distinct from that of the summer North Atlantic Oscillation, despite the two modes of variability bear strong similarities in their upper level

atmospheric pattern over Western Europe. The analysis of simulated CGT features and of its climatic implications for the European region substantiates the existence of the CGT-European summer precipitation connection. The summer CGT in the mid-latitude therefore adds to the list of the modes of large-scale atmospheric variability significantly influencing European summer precipitation variability.

**Keywords** European summer precipitation · Circumglobal wave train · Summer North Atlantic Oscillation

## 1 Introduction

European summer precipitation variability substantially affects human activities on the continent on a broad range of time scales, ranging from intraseasonal to interannual and decadal ones. Both enhanced and deficient summer rainfall can lead to serious social and economic consequences and to significant damage to regional economies (e.g., Christensen and Christensen 2003; Schär et al. 2004; Marsh and Hannaford 2007; Blackburn et al. 2008, Lenderink et al. 2009). During the recent decades considerable extreme weather/climate events impacted on the European region during the summer season. An example of such extremes is the anomalously high precipitation over Great Britain during summer 2007 that resulted in extensive flash flooding across England and Wales (Marsh and Hannaford 2007; Blackburn et al. 2008).

Both land surface processes (Koster and Suarez 1995a, b; Schär et al. 1999; Seneviratne et al. 2006) and atmospheric circulation (Pal et al. 2004; Koster et al. 2004; Ogi et al. 2005) contribute modulating European summer

S. Saeed (✉) · N. Van Lipzig  
Department of Earth and Environmental Sciences, KU Leuven,  
Leuven, Belgium  
e-mail: saeed.saeed@ees.kuleuven.be

W. A. Müller · D. Zanchettin  
Max Planck Institute for Meteorology, Hamburg, Germany

F. Saeed  
Climate Service Center, Helmholtz-Zentrum Geesthacht,  
Hamburg, Germany

precipitation. In fact, compared to moisture advection, local land surface processes become more important for precipitation in the summer season (Trenberth 1999). Moreover, warmer sea surface temperature (SST) anomalies in the tropical and North Atlantic could be associated with warmer and moister air, thereby influencing downstream precipitation over land after advection. Since the above mechanisms are not mutually exclusive, there is a high degree of uncertainty regarding their individual role in summer precipitation variability in the northern hemisphere extra-tropics and particularly over Europe.

Predictability of mid-latitude climates is limited for the summer compared to the winter season (e.g., Dirmeyer et al. 2003; Koenigk and Mikolajewicz 2008). This statement particularly applies to the European region, despite the efforts devoted at understanding and predicting its summer climate variability (e.g., Colman and Davey 1999; Hurrell and Folland 2002; Zvereva 2004; Zolina et al. 2008). Colman and Davey (1999) found quite low prediction skills of statistical models of the European summer climate on the basis of an analysis of the North Atlantic SST anomalies. On the other hand, initialization has been shown to improve the forecast skill of a dynamical prediction system for yearly and multi-yearly means predominately over the North Atlantic, which contributes to the positive skill scores for summer means over central and south-eastern Europe (Müller et al. 2012). Ground for improved understanding of European seasonal climate variability is provided by the identification of strongly influential large-scale modes of atmospheric variability. This is certainly the case of the winter North Atlantic Oscillation (NAO), which is the leading mode of winter atmospheric variability in the northern hemisphere and the dominant factor controlling European winter precipitation variability (e.g., Hurrell 1995; Qian et al. 2000; Zvereva 2006; Zanchettin et al. 2008). Although of lesser amplitude than its wintertime counterpart, the SNAO exerts a similarly strong influence on northern European summer rainfall, temperature, and cloudiness through changes in the position of the North Atlantic storm track (e.g., Folland et al. 2009; Bladé et al. 2011). It remains nonetheless an open question whether and how other modes of large-scale atmospheric variability impact European summer precipitation.

Branstator (2002) noticed that low frequency disturbances in the vicinity of the subtropical jet stream stretching across South Asia are meridionally trapped and zonally elongated during the winter season. One special phase of this pattern co-vary with distant regions in mid-latitudes producing a pattern of variability known as the CGT pattern. Previous studies (e.g., Ding and Wang 2005; Saeed et al. 2011a, b) have shown that the CGT affects northern hemisphere regional summer climates by modulating the Asian summer monsoon. Here we show that a

similar CGT wave-like pattern is consistently found in NCEP/NCAR reanalysis and ECHAM6/MPIOM model data, and further explore its regional implications for the European summer climate on inter-annual time scales. In particular, we use synthesis (reanalyzed) climate data to demonstrate that the CGT is linked to European summer precipitation via a mechanism involving the upper and lower level circulation over the European region. To compensate for the temporal limitedness of reanalysis data, we additionally investigate the CGT–European summer precipitation relationship in a historical climate simulation carried out with the ECHAM6/MPIOM coupled general circulation model. The paper is organized as follows. Section 2 describes the data and methods used in this study; Sect. 3 illustrates the connection between the CGT and European summer climate as detected in the NCEP/NCAR reanalysis data. Section 4 provides an overview of the distinguishing traits between CGT and SNAO. The CGT link with European summer precipitation as detected in the reanalysis data is detailed in Sect. 5. An analysis of the ECHAM6/MPIOM simulation is presented in Sect. 6. A summarizing discussion concludes the paper.

## 2 Data and methodology

### 2.1 Data

#### 2.1.1 Datasets and model description

The main analysis is carried out on NCEP/NCAR reanalysis monthly-mean fields (Kalnay et al. 1996). We further use the observational gridded 0.25°E-OBS precipitation data, which represent the most complete and corrected European climate dataset (Haylock et al. 2008). SST data are from the monthly Kaplan extended SST V2 dataset, which extends back to 1856 (Kaplan et al. 1998). We also used NOAA high resolution daily SST data for the period 1982–2010 (Reynolds et al. 2007). A low signal-to-noise and/or limited representativeness due to paucity of relevant episodes during the observed period may affect the generality of our conclusions. To increase confidence on our observational-based inferences, we therefore additionally perform an analogous analysis on a historical climate simulation (1901–2005) carried out using the coupled ECHAM6/MPIOM climate model. The simulation contributes to the fifth phase of the Coupled Model Inter-comparison Project (CMIP5) (Taylor et al. 2012). A detailed description of the ECHAM6/MPIOM model is given by Giorgetta et al. (2012) and Jungclaus et al. (2013). ECHAM6 is run at T63 horizontal resolution and 47 vertical levels extending up to 0.01 hPa, therefore allowing for an improved representation of stratospheric processes and

of stratospheric/tropospheric interactions. MPIOM is run in the GR15L40 configuration, corresponding to a horizontal resolution ranging between 12 and 180 km. Despite representing a major advance compared to its previous generation counterpart, ECHAM6/MPIOM still features a cold SST bias covering the region surrounding the subtropical gyre margin, likely due to lack of resolution preventing a proper representation of the Gulf Stream separation (Jungclaus et al. 2013).

Pre-processing includes de-trending of the monthly datasets and computation of the July–August anomalies by removing the corresponding long-term climatological mean value from each monthly-mean series.

### 2.1.2 Indices

The circumglobal mid-latitude wave train index (CGTI) is defined as the principal component associated to the first empirical orthogonal function (EOF) of northern hemisphere summer (July–August) 200 hPa meridional wind anomalies (Ding and Wang 2005). Here, the CGT is extracted over the domain [20°N–80°N; 100°W–100°E] following Saeed et al. (2011a). Following Folland et al. (2009), we also define the SNAOI index (SNAOI) as the leading EOF (explained variance 29 %) of summer (July–August) mean sea level pressure (MSLP) over the region [25°N–70°N, 70°W–50°E]. We also define Western Europe precipitation indices for CGT (hereafter WEPI-CGT) and SNAOI (hereafter WEPI-NAO) to examine the integrated response of regional precipitation to the large scale circulation anomalies. Specifically, WEPI-CGT is defined as the difference of area averaged precipitation between western [45°N–50°N; 0°E–30°E] and eastern [55°N–65°N; 30°E–60°E] Europe. WEPI-NAO is defined as the difference of area averaged precipitation between northern [50°N–60°N; 10°W–35°E] and southern [40°N–45°N; 10°W–35°E] Europe. A small change in the area averages used to define the above indices does not appreciably influence the results. For both the reanalysis and the simulated data, the indices are defined for the period 1950–2010 and are summarized in Table 1.

**Table 1** Indices acronyms and their definitions

Index	Definition
CGTI	The principal component associated to the first empirical orthogonal function (EOF) of northern hemisphere summer (July–August) 200 hPa meridional wind anomalies over the domain [20°N–80°N; 100°W–100°E].
SNAOI	The principal component associated to the first empirical orthogonal function (EOF) of summer (July–August) MSLP over the region [25°N–70°N, 70°W–50°E]
WEPI-CGT	The difference of area averaged precipitation between western [45°N–50°N; 0°E–30°E] and eastern [55°N–65°N; 30°E–60°E] Europe
WEPI-NAO	The difference of area averaged precipitation between northern [50°N–60°N; 10°W–35°E] and southern [40°N–45°N; 10°W–35°E] Europe

A preliminary analysis was performed to assess the implications of different definitions of the CGTI, specifically based on single months (i.e., July and August individually) and bimonthly (i.e., July–August) mean. Differences between single-month and bimonthly CGTI estimates are overall marginal over the investigated period. The only appreciable difference lies in the percentage of total variance explained by the index, which ranges between 15.2 % for the single-month index and 18.2 % for the bimonthly index. In the following, we opt for the monthly pattern as this allows assessing the month-by-month contribution of the CGT to the seasonal field anomalies.

### 2.1.3 Composite analysis

The CGTI, SNAOI, WEPI-CGT and WEPI-NAO are used as grouping variables in a composite analysis. The grouping criterion separates positive and negative values of CGTI and SNAOIs based on exceedance of the  $\pm 1$  SD thresholds (in-between values correspond to a neutral state of the index). Similarly, the grouping criterion separates positive WEPI-CGT and WEPI-NAO anomalies based on exceedance of the  $\pm 1$  mm thresholds (in-between values correspond to a neutral state of the index). Here, the composite anomalous fields are calculated as differences between the positive-average and the neutral-average case for the positive composite (referred to as positive phase), and between the negative-average and the neutral-average case for the negative composite (referred to as negative phase). We applied a *t* test to estimate the statistical significance of the correlations and composites.

## 3 Relevance of the observed CGT to European summer climate

Figure 1 illustrates the CGTI (panel b) and associated EOF pattern (panel a) calculated from reanalysis data of 200 hPa meridional wind anomalies. The EOF pattern entails a wave-like structure similar to the CGT extending well into

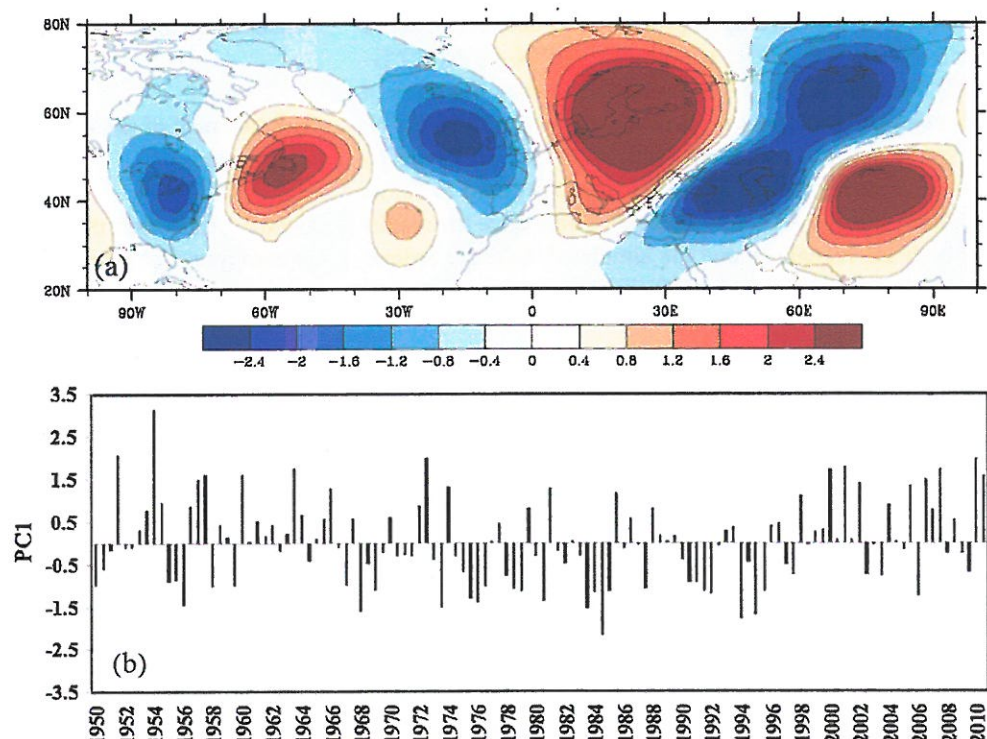
the North-Atlantic-European region. The CGTI time series displays pronounced month-by-month as well as inter-annual variability. Negative values of the index are predominant during the period between about 1975 and 1997, while positive values predominate thereafter, suggesting that multidecadal variability also contributes to the index's evolution.

The 200 hPa geopotential height composites using CGTI reveal a wave like pattern extending from the North Pacific to Eurasia (Fig. 2a, b). The positive CGT phase is associated with upper level anomalous low (high) pressure over western (eastern) Europe (Fig. 2a). The anomalous patterns associated with positive CGT phase display strong signals over the eastern US, the North Atlantic and Eurasia. The signals are weak and insignificant to the west of 100°W (Fig. 2a). The circulation pattern over the North Atlantic and Eurasia region inverts for the negative phase of the CGT (Fig. 2b). CGT significantly and extensively imprint also at the surface levels as shown by the MSLP pattern in Fig. 2c, d. During the positive CGT phase, the MSLP fields display a wave-like pattern with significant low and high pressure anomalies extending from the North Pacific to Eurasia (Fig. 2c). In particular, it is associated with an anomalous low pressure center over the sub-polar gyre region in the North Atlantic and with an anomalous high pressure center over the Baltic Sea and Eastern Europe. During the negative phase the anomalous MSLP pattern entails, as main feature, a low pressure center located

over the North Sea and extending south-westward (Fig. 2d). Overall, CGT significantly imprints on both upper and surface atmospheric circulation with a wave-like pattern. Composite analysis reveals some non-linearity in this imprint: the anomalies stretch hemispherically during positive CGT phases, while they are more apparently confined in the Euro-Atlantic/western Russian region during negative CGT phases. Moreover, the centers of the anomalies do generally not correspond during positive and negative CGT phases.

The SST anomalies associated with the positive CGT phase reveal anomalously warm conditions in the western subtropical and North Atlantic Ocean along the Gulf Stream trajectory (Fig. 3a). Warm SST anomalies emerge also in the tropical and equatorial Atlantic, and in the Indo Pacific warm pool region. During the negative CGT phase the SST anomalies display significant cold conditions in the North Pacific and the central North Atlantic Ocean (Fig. 3b). Especially, SSTs in the Gulf of Mexico appear as a potentially important factor implicated in the diagnosed atmospheric signature of CGTI. To clarify this, we calculate the average SST over the domain [90°W–70°W; 15°N–30°N] and correlate it to the northern hemispheric MSLP field. Significant negative correlations are found over the US and Europe, while positive correlation spread over the Arctic and the tropical Pacific (Fig. 4a). The negative correlation indicates that the enhanced (reduced) SST anomalies in the western subtropical Atlantic along the

**Fig. 1** By using the NCEP reanalysis data, **a** Leading first EOF mode of 200 hPa meridional wind, **b** first principal component associated with leading EOF mode. The leading EOF mode explains 15.2 % of the total variance and reveals a wavelike pattern similar to mid-latitude circumglobal wave train. EOFs are computed over the region [100°W–100°E, 20°N–80°N] using the departures of 200 hPa mean meridional wind for July–August from 1950 to 2010



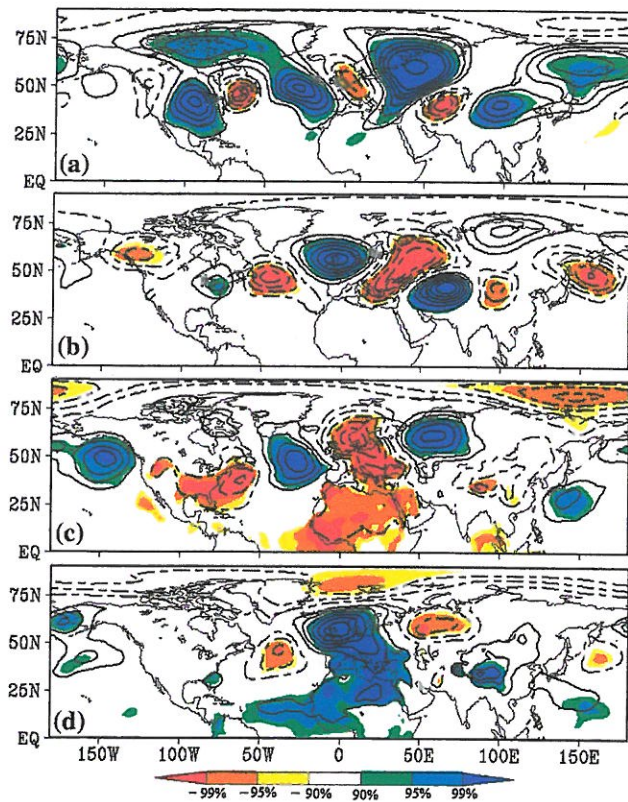


**Fig. 2** Composite difference of 200 hPa geopotential height for a CGTP – neutral, b CGTN – neutral. The composite are based on the first principal component (CGTI) of the wave train shown in Fig. 1b. CGTP (CGTN) refers to the cases when CGTI is *above* (+1) (*below* -1) SD. Between  $\pm 1$  SD, the period is considered as neutral. c, d Same as a, b except for MSLP. The contours interval in a, b (c, d) is 10 gpm (0.5 hPa) and the zero contour line is omitted. The negative contours are shown by the dashed line. Shaded areas shows the differences that are significant to  $\pm 90$ ,  $\pm 95$  and  $\pm 99$  % significance level

southeastern US coast and the Gulf of Mexico is associated with low level anomalous low (high) pressure over the US and the western European region.

An analogously defined regional-average [ $90^{\circ}\text{W}$ – $70^{\circ}\text{W}$ ,  $15^{\circ}\text{N}$ – $30^{\circ}\text{N}$ ] MSLP (hereafter SLPI) significantly correlates with 200 hPa geopotential height and meridional wind anomalies producing a CGT-like wave pattern in the mid-latitudes, especially over Eurasia (Fig. 4b, c). A one point correlation map between SLPI with 200 hPa geopotential heights further shows a northward extension of negative correlations over the US and the North Atlantic region (shown by the northward pointing arrows in Fig. 4b). In particular, SLPI positively correlates with 200 hPa geopotential heights over Western Europe indicating that a decrease in MSLP in the western subtropical Atlantic along the south-eastern US coast may be associated with a decrease in 200 hPa geopotential height above western Europe.

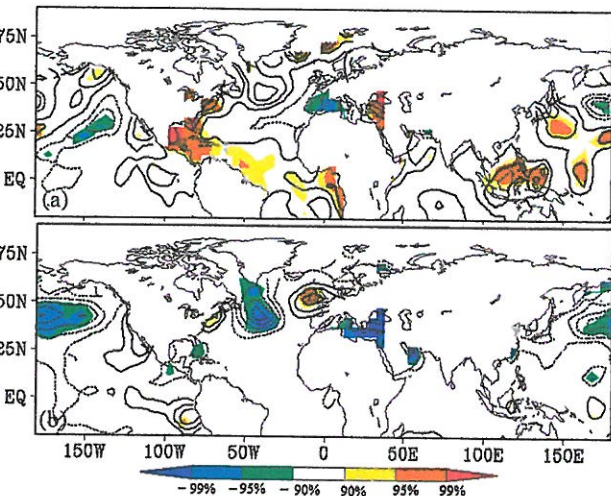


**Fig. 3** Same as Fig. 2a, b except for sea surface temperature (contours). Negative contours are shown by dashed lines. Contours are plotted at  $0.1^{\circ}\text{C}$  interval and zero contour line is omitted. Shaded areas shows the differences that are significant to  $\pm 90$ ,  $\pm 95$  and  $\pm 99$  % significance levels

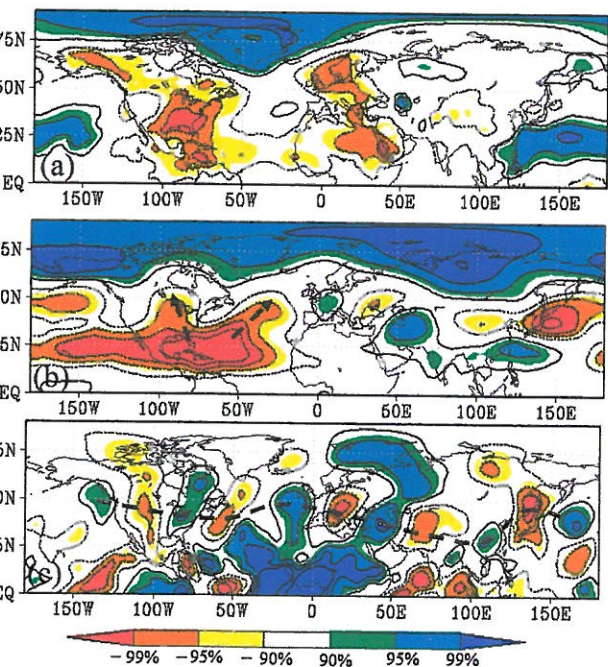


**Fig. 4** One point correlation map between a area averaged SST anomalies over [ $90^{\circ}\text{W}$ – $70^{\circ}\text{W}$ ,  $15^{\circ}\text{N}$ – $30^{\circ}\text{N}$ ] and SLP, b SLPI and 200 hPa geopotential heights, c SLPI and 200 meridional wind. SLPI refers to the area averaged MSLP over region [ $90^{\circ}\text{W}$ – $70^{\circ}\text{W}$ ,  $15^{\circ}\text{N}$ – $30^{\circ}\text{N}$ ]. The two arrows in b show northward extension of negative correlations over the US and the North Atlantic Ocean. The dashed line in c shows a wavelike pattern extending well in the in mid-latitudes

However, it is not clear from the correlation analysis which system may lead the other. We therefore carried out a lead-lag relationship between the daily SST averaged over western subtropical Atlantic [ $90^{\circ}\text{W}$ – $70^{\circ}\text{W}$ ,  $15^{\circ}\text{N}$ –

$30^{\circ}\text{N}$ ] and 200 hPa geopotential heights above western Atlantic [ $40^{\circ}\text{W}$ – $70^{\circ}\text{W}$ ;  $25^{\circ}\text{N}$ – $45^{\circ}\text{N}$ ] and Eastern Atlantic [ $0^{\circ}\text{W}$ – $30^{\circ}\text{W}$ ;  $25^{\circ}\text{N}$ – $45^{\circ}\text{N}$ ] for the period 1982–2010 (Fig. 5). It can be seen that the SST leads the 200 hPa geopotential height above Atlantic Ocean by several days. A plausible mechanism describing how warm SST in the western subtropical Atlantic can influence the precipitation over Europe is as follows: first, the warm SST anomalies in the western subtropical Atlantic is associated with deepening of low pressure over the south-eastern US and adjacent areas. The intensification of the anomalous low pressure favors strong moisture convergence and associated precipitation over this region. The enhanced precipitation and associated latent heat release above this region (Hodson et al. 2010) may influence the upper level circulation that propagates eastward and modulates precipitation over the European region. The 200 hPa geopotential height composites show strong upper level signals above this region (around  $100^{\circ}\text{W}$  and  $40^{\circ}\text{N}$ ) during the positive CGT phase (Fig. 2a), further supporting this hypothesis. To the west of  $100^{\circ}\text{W}$ , the wave like signals are weak and non significant. The suggested mechanism for the SST-CGT connection is similar to that shown by Saeed et al. (2011b) for the Asian monsoon region. Saeed et al. (2011a) showed that the eastward propagation of the wave train may influence the MSLP and associated precipitation over northwestern India and Pakistan. Since the anomalous MSLP anomalies over the Atlantic-European region are consistent with the atmospheric circulation anomalies associated with the CGT, the alternative hypothesis cannot be ruled out that the SST anomalies in the subtropical Atlantic could be a response of the circulation anomalies. Further investigations based on sensitivity model experiments (e.g., Rodwell et al. 2004; Saeed et al. 2011b) are needed to clarify the role of the warming in the subtropical Atlantic and the proposed feedback mechanism.

#### 4 Difference between CGT and other modes

The SNAO is a prominent feature of summer atmospheric variability in the North Atlantic/European sector. It is therefore natural to ask the question to what extent the upper and low level signals associated with the summer CGT over the North Atlantic and European region differ from that of the SNAO. A detailed description of the SNAO and its associated influence on the European summer climate is given by Folland et al. (2009) and Bladé et al. (2011). The anomalous MSLP pattern associated with SNAOI reveals strong anticyclonic (cyclonic) circulation over the UK and northwestern Europe (Greenland) during the positive phase (not shown). Variations in the SNAO are associated with changes in the North Atlantic storm track,

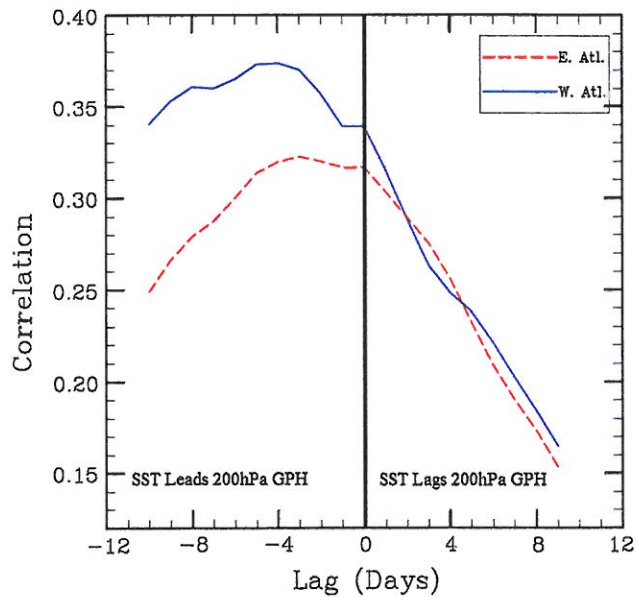


**Fig. 5** Lead–lag relationship between area averaged sea surface temperature over western subtropical Atlantic [ $15^{\circ}\text{N}$ – $30^{\circ}\text{N}$ ;  $90^{\circ}\text{W}$ – $70^{\circ}\text{W}$ ] and 200 hPa geopotential height above western [ $25^{\circ}\text{N}$ – $45^{\circ}\text{N}$ ;  $70^{\circ}\text{W}$ – $40^{\circ}\text{W}$ ] and eastern [ $25^{\circ}\text{N}$ – $45^{\circ}\text{N}$ ;  $0^{\circ}$ – $30^{\circ}\text{W}$ ] Atlantic Ocean

cloudiness surface temperature and rainfall (Folland et al. 2009). SNAO reveals an opposite response compared to CGT on the upper levels and surface precipitation. In order to make SNAO plots homogenous to CGT, we show here the reverse response of SNAO to the upper troposphere i.e., the composite difference of negative (positive) SNAOI below  $-1$  (above  $+1$ ) SD – neutral cases [cases for which SNAOI values lies between  $\pm 1$  SD] and is referred to as negative (positive) SNAO phase respectively.

The 200 hPa geopotential height anomalies associated with SNAO (Fig. 5a, b) and CGT (Fig. 2a, b) bear similarities over the western European region, but the two modes display distinct features in the entire northern hemisphere. The 200 hPa geopotential height pattern associated with SNAO reveals a north–south dipole like pressure patterns over Europe (Folland et al. 2009). The negative (positive) SNAO phase is associated with upper level anomalous low (high) over northwestern Europe and high (low) over Mediterranean region (Fig. 6a, b). Compared to SNAO, the CGT mode displays an east–west dipole like pattern (Fig. 2a, b). Moreover, SNAO displays strong signals over the US, North-Atlantic and European region (Fig. 6a, b), whereas the CGT pattern extends throughout the entire northern hemisphere (Fig. 2a, b).

The MSLP anomalous patterns associated with SNAO (Fig. 6c, d) and CGT (Fig. 2c, d) reveal differences between the two modes. The precipitation associated with SNAO (not shown) entail a north–south dipole like pattern (Folland et al. 2009) with enhanced (suppressed) precipitation over northern Europe (Mediterranean region) during

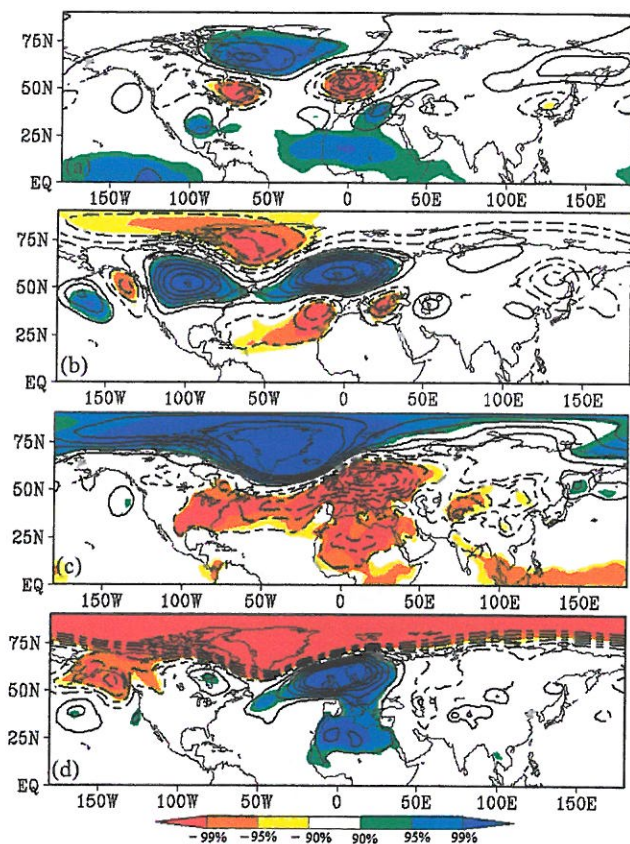


**Fig. 6** a, b Composite difference of 200 hPa geopotential height between a negative SNAOI and neutral, b positive SNAOI and neutral. Positive (negative) SNAOI refers to the cases for which SNAOI is above +1 (below -1) SD. Between  $\pm 1$  SD, the SNAOI cases are considered as neutral. c, d Same as a, b except for MSLP. The contours interval in a, b (c, d) is 10 gpm (0.5 hPa) and the zero contour line is omitted. Negative contours are shown by the dashed line. Shaded areas show the differences that are significant to  $\pm 90$ ,  $\pm 95$  and  $\pm 99$  % significance levels

the negative (positive) SNAO phase. The CGT, by contrast displays an east–west dipole-like precipitation pattern over Europe (discussed in the next section). Not only the patterns differ between the two modes, the correlations between CGTI and SNAOI ( $r = 0.2$ ) and is not significant, and rather points towards linear independence between the two modes. It is not clear yet whether the evolution of the two modes on sub-seasonal time scales is interrelated i.e., if the early onset of an anomalous state in one of the modes could trigger an analogous anomalous phase of the other one. On the other hand both indices (i.e., CGTI and SNAOI) display significant correlations with European summer precipitation, but with different portion of its variability (Fig. 7). This further suggests that the European summer precipitation is differently influenced by both modes of the mid-latitude atmospheric variability.

We also investigated possible repercussions of the El Niño Southern Oscillation (ENSO) on the observed

relationship between CGT and summer European precipitation by excluding from the composite analysis those years characterized by strong El Niño or La Niña episodes. Since the obtained patterns for non-ENSO cases do not differ substantially from the full-period analysis (results not shown), we conclude that the CGT-European summer precipitation relation is not significantly influenced by ENSO. Our results are in agreement with previous indications that the summer CGT is independent of ENSO (Ding and Wang 2005).

## 5 CGT impacts on European summer precipitation

We have seen that the positive phase of CGT is associated with upper level anomalous low (high) pressure over western (eastern) Europe. The composite analysis reveals significantly enhanced (reduced) summer precipitation over western (eastern) Europe during the positive CGT phase and vice versa for the negative phase (Fig. 8a, b). It can be seen that the CGT is associated with linear east–west dipole-like precipitation pattern over Europe. During the positive phase of the CGT the anomalous low pressure that develops over Western Europe (Fig. 2a, c) favors strong moisture convergence over this region. The anomalous low pressure is further associated with enhanced convection and associated precipitation over Western Europe. On the other hand, the anomalous high pressure over Eastern Europe suppresses the convection and associated precipitation over Eastern Europe and thus favors a dipole-like precipitation pattern over Europe (Figs. 2a, c, 8a). A reverse occurs during the negative phase of the CGT (Figs. 2b, d, 8b).

In order to further improve our confidence on the above results, we examined the large scale circulation response associated with enhanced summer precipitation over western (northern) Europe. For this purpose we carried out a composite analysis using the WEPI-CGT and WEPI-NAO indices as defined in Sect. 2. A positive WEPI-CGT (WEPI-NAO) phase refers to an enhanced precipitation over western (northern) Europe compared to eastern (southern) Europe. There is no statistically significant correlation between WEPI-CGT and WEPI-NAO. Moreover, a small change in the area averages used to defined WEPI-CGT and WEPI-NAO do not appreciably affect the results.

The relation between the European precipitation indices and the upper troposphere is shown in Fig. 9. The 200 hPa geopotential height composites associated with the positive WEPI-CGT phase reveal a well defined wavelike pattern (Fig. 9a) similar to that for a positive CGT phase (Fig. 2a) extending from North Pacific to Eurasia. To the west of 100°W, the signals associated with positive WEPI-CGT

**Fig. 7** Scatter plot of (left) CGTI and WEPI-CGT (right) SNAOI and WEPI-NAO. The correlation between the two indices is shown in the upper left corner

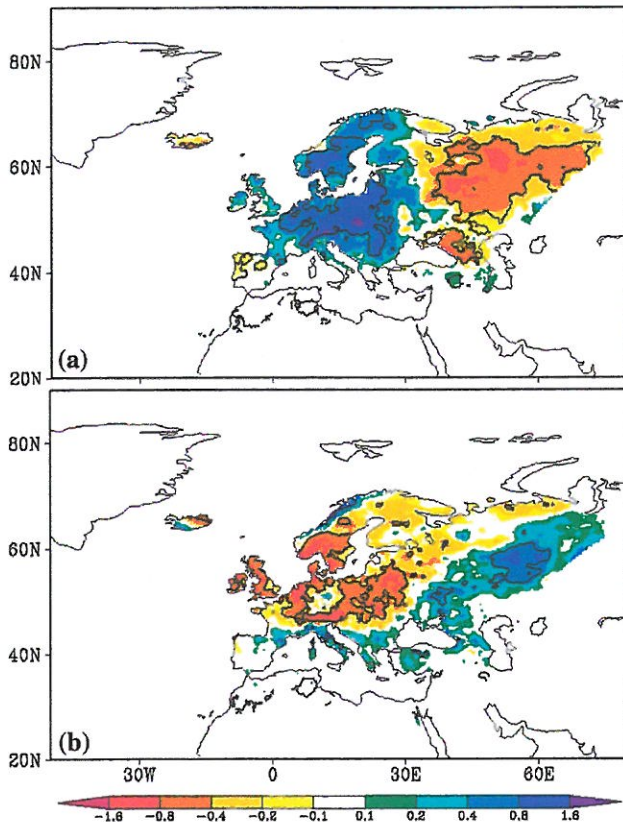
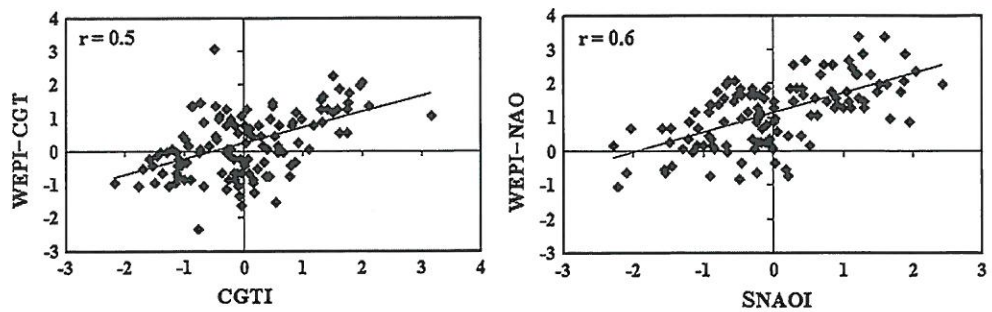


**Fig. 8** Same as Fig. 2a, b except for precipitation. The contour line shows the differences that are significant to 95 % level. The unit of precipitation is  $\text{mm day}^{-1}$

phase are weak and non significant, which is again similar to the positive CGT phase shown in Fig. 2a. At lower levels, the MSLP associated with the positive WEPI-CGT phase reveals significantly low pressure anomalies over western Europe, the tropical Atlantic, the southeastern US coast and the Gulf of Mexico together with high pressure anomalies over northeastern Europe, the North Atlantic and the north-eastern US (Fig. 9b). With some exceptions the MSLP pattern associated with positive WEPI-CGT phase over the European region resembles to that shown in Fig. 2b. In the US, Gulf of Mexico and tropical Atlantic region the MSLP pattern associated with positive WEPI-CGT phase resembles to the one point correlation map

between SST and MSLP shown in Fig. 4a. Moreover, similar to the CGT the 200 hPa geopotential height anomalies associated with the positive WEPI-CGT phase show significantly strong signals to the east of 100°W. This further supports the hypothesis that the enhanced SST in the western subtropical Atlantic along southeastern US coast and the Gulf of Mexico may trigger the positive CGT phase and associated precipitation over Europe.

We further examined the upper level 200 hPa geopotential height and MSLP associated with the positive WEPI-NAO phase (Fig. 9c, d). Both the upper level 200 hPa geopotential height and lower level MSLP associated with the positive WEPI-NAO phase resemble to the SNAO associated patterns shown in Fig. 6a, c. As discussed earlier the WEPI-CGT and WEPI-NAO indices are not significantly correlated. CGT correlates significantly with both WEPI-CGT ( $r = 0.5$ ) and WEPI-NAO ( $r = 0.38$ ). On the other hand SNAOI displays significant correlation ( $r = 0.6$ ) with WEPI-NAO, but very weak and non significant correlations ( $r = 0.1$ ) with WEPI-CGT. This indicates that the SNAO is predominantly associated with north-south dipole-like precipitation pattern. By contrast, CGT is predominantly associated with an east-west precipitation pattern over Europe. Although, CGT and SNAO bear some similarities in their upper level signature above western Europe, nevertheless the two modes have distinct influences on the European summer precipitation.

## 6 ECHAM 6/MPIOM simulation

Several climate model simulations for the twenty-first century project pronounced decrease in summer precipitation over Europe and the Mediterranean region (Meehl et al. 2007). However, this agreement between the models does not prove the realism of the mechanisms involved in the summer drying over Europe. One way to increase our confidence in these model projections is to examine whether the large-scale dynamical mechanisms that influence summer precipitation in Europe are well represented in the models. For this purpose, we examined the ECHAM6/MPIOM climate simulations for the twentieth century

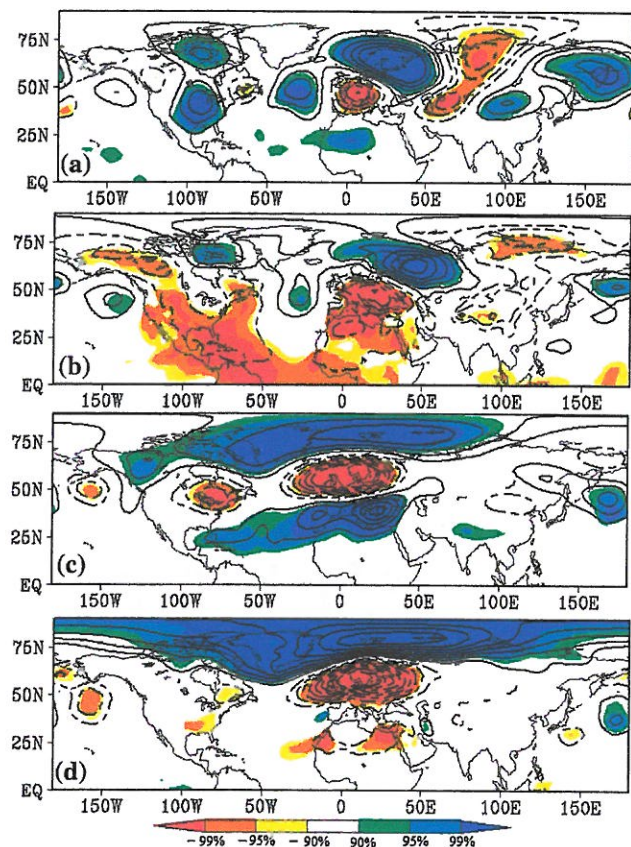


**Fig. 9** By using WEPI-CGT the composite difference of a 200 hPa geopotential height, **b** mean sea level pressure. A composite difference is simply the positive WEPI-CGT (*above* +1 mm) – neutral cases (cases for which WEPI-CGT lies between  $\pm 1$  mm). **c, d** Same as **a, b** except for WEPI-NAO. The contours interval in **a–c** (**b–d**) is 10 gpm (0.5 hPa) and the zero contour line is omitted. Negative contours are shown by the dashed line. Shaded areas show the differences that are significant to  $\pm 90$ ,  $\pm 95$  and  $\pm 99$  % significance levels

(1901–2005). On the same lines as for NCEP/NCAR reanalysis data, we analysed the proposed mechanism using ECHAM6/MPIOM simulations. The objective here is not a one-to-one comparison between model and observations/reanalysis datasets but is to see the extent to which model simulates the proposed large scale teleconnection pattern that influence precipitation over Europe.

We first computed the EOFs using the 200 hPa meridional wind anomalies over the same domain as used for NCEP/NCAR reanalysis data. The first leading mode the EOF display a wave-like pattern similar to CGT (Fig. 10a) as seen in case of NCEP reanalysis datasets (Fig. 1a). Similar to the NCEP/NCAR reanalysis data we carried out a composite analysis using the first principal component (CGTI) of the leading first EOF mode. The 200 hPa geopotential height composites using simulated CGTI display a wave like pattern in the mid-latitudes extending from the North Pacific to Eurasia region (Fig. 11a, b). The simulated

200 hPa geopotential height pattern associated with CGT resembles to that of NCEP/NCAR reanalysis over the European region (Figs. 2a, b, 11a, b); however, considerable differences can be seen above the US and the North Pacific region. It is interesting that the model simulation depicts reasonably well the upper level anomalous low (high) over the western (eastern) European region during the positive and negative phase of CGT. At lower levels the simulated MSLP composites manifest the anomalous low (high) over western Europe during the positive (negative) phase of CGT (Fig. 11c, d). In the North Atlantic-European sector the simulated MSLP composite pattern resembles the NCEP reanalysis data (Figs. 2c, d, 11c, d). The model simulated reasonably well the anomalous low pressure over the western subtropical Atlantic Ocean during the positive CGT phase (Fig. 11c).

It is further interesting that the ECHAM6/MPIOM model simulates reasonably well the east–west dipole like precipitation pattern associated with the CGT over European region (Fig. 12a, b). The simulated precipitation composites do not exactly superpose on the observed pattern, especially for the positive phase of CGT, but in general the model capture reasonably the observed CGT features and associated European summer precipitation (Fig. 12a, b). For positive CGT phase the simulated precipitation composite display a mixed CGT and SNAO like pattern compared to observations. Similar to the observational and reanalysis data we also defined precipitation indices (WEPI-CGT and WEPI-NAO) using the simulated precipitation. The composites associated with the WEPI-CGT (WEPI-NAO) reveal CGT (SNAO) like patterns in the upper troposphere in the northern hemisphere (not shown). Furthermore, the simulated precipitation anomalies are consistent with the circulation anomalies, further suggesting that the model is able to capture the basic proposed mechanism.

## 7 Summary and conclusions

We examined the European summer precipitation variability and associated teleconnections using the NCEP/NCAR reanalysis and a historical CMIP5 climate simulation performed with the ECHAM6/MPIOM climate model. Special emphasis is given to the summer circumglobal wave train (CGT), which is known to influence the mid-latitudes regional climates and especially the Asian summer monsoon (Ding and Wang 2005; Saeed et al. 2011a). We found a wavelike pattern in the upper tropospheric levels similar to the mid-latitude CGT extending from the North Pacific to Eurasia (Figs. 1a, 2a, b). The positive phase of the CGT is associated with upper level anomalous low (high) pressure over western (eastern) Europe

**Fig. 10** Same as Fig. 1 except using ECHAM6/MPIOM data

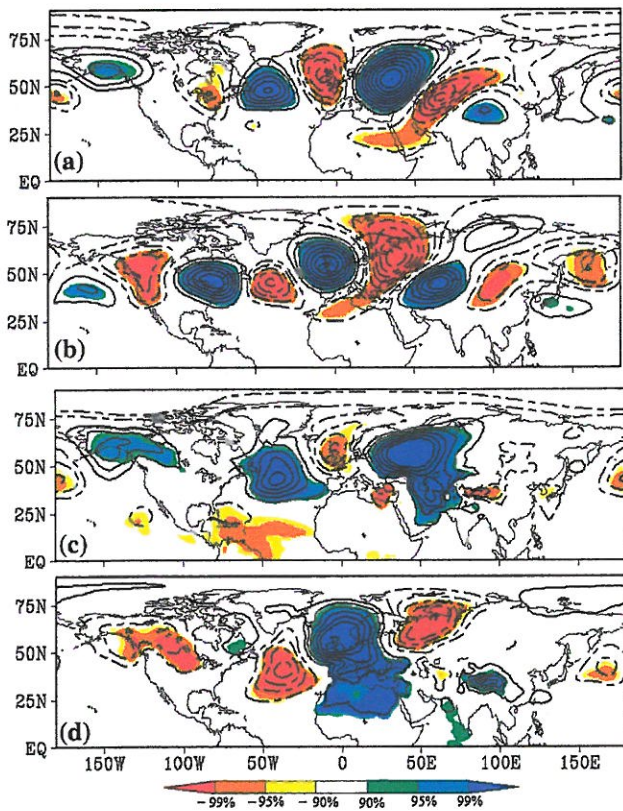
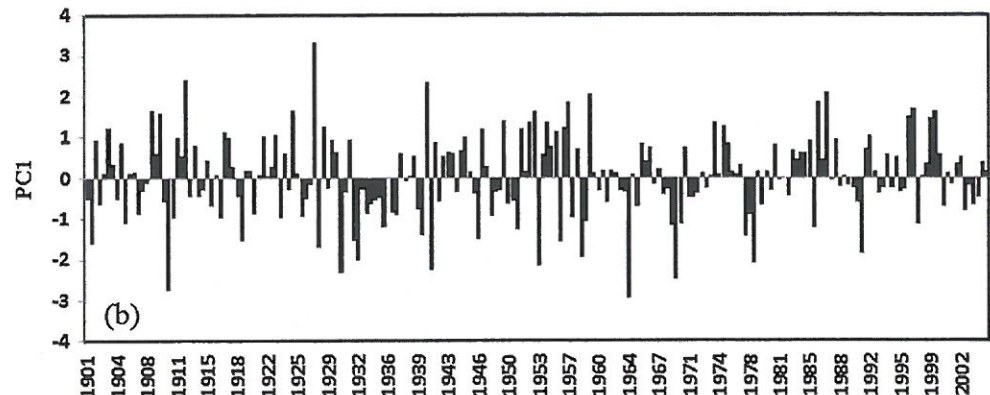
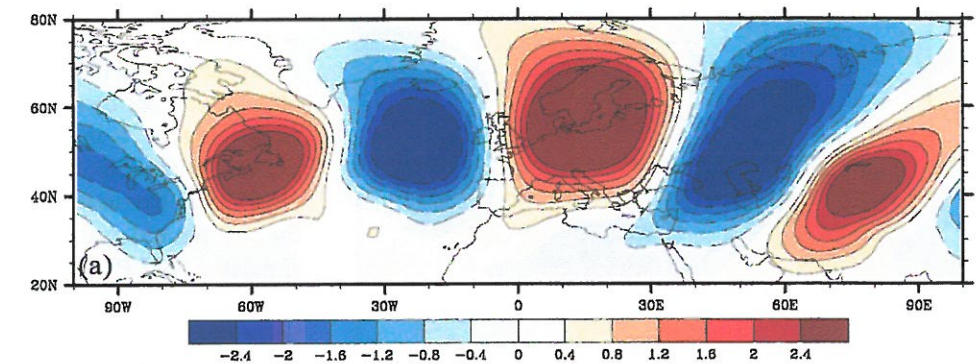


**Fig. 11** Same as Fig. 2 except using ECHAM6/MPIOM data

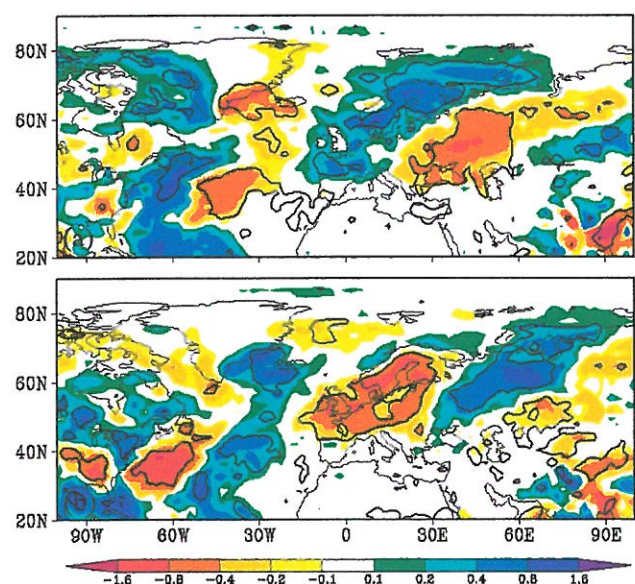


**Fig. 12** Same as Fig. 8 except using ECHAM6/MPIOM data

(Fig. 2a). At lower levels the MSLP field displays significant low (high) pressure anomalies over western (eastern) Europe (Fig. 2c). The positive phase of the CGT is further associated with enhanced (reduced) precipitation over western (eastern) Europe and display an east–west dipole

like pattern (Fig. 8a). The circulation and associated precipitation patterns over Europe grossly invert for the negative phase of CGT (Figs. 2b, d, 8b). The composite analysis reveals, however, some non-linearity in the CGT imprint on both upper and surface atmospheric circulation in the entire northern hemisphere.

The European summer precipitation is known to be strongly influenced by the SNAO (e.g., Folland et al. 2009; Bladé et al. 2011). We also assessed the differences between the imprints of the CGT and the SNAO on European summer precipitation. SNAO is associated with a north–south dipole-like precipitation pattern over Europe (Folland et al. 2009; Bladé et al. 2011), whereas CGT is associated with an east–west dipole-like pattern (Fig. 8). Furthermore, the anomalous patterns associated with the two modes bear some similarities in the upper level above western Europe, but the two modes manifest distinct features at the hemispheric scale (Figs. 2, 6).

In order to examine the robustness of the CGT-European summer precipitation linkage described above we also performed a “reverse” analysis by investigating large-scale circulation anomalies associated with meridional (namely WEPI-CGT) and with a zonal (WEPI-NAO) precipitation anomalous dipole pattern in European precipitation. The indices associated to the two precipitation patterns are defined to be in a positive phase for enhanced (reduced) precipitation over western (eastern) Europe (WEPI-CGT) and for enhanced (reduced) precipitation over northern (southern) Europe (WEPI-NAO). The 200 hPa geopotential height anomalies associated with a positive WEPI-CGT phase reveals CGT like wave pattern in the mid-latitudes (Fig. 9a). The upper level response associated with positive WEPI-NAO phase displays SNAO like pattern over Euro-Atlantic region (Fig. 9c). The anomalous MSLP pattern associated with the positive WEPI-CGT phase displays significant anomalies that stretch hemispherically, whereas it is more localized and reveals SNAO like pattern for the positive WEPI-NAO phase (Fig. 9b, d). Overall, using the WEPI indices as grouping variables the gross large-scale circulation features associated to the CGT and the SNAO can be retrieved. We are therefore confident, in particular, that the described CGT-European summer precipitation linkage is not spurious but, indeed, describes a causal relationship. Although, the CGT and the SNAO share some similarities in the upper level (200 hPa geopotential height) signature over western Europe, nevertheless, the two modes have distinct imprints on the European summer precipitation.

To further increase our confidence on the observational-based inferences, we additionally performed an analysis on a historical (1901–2005) CMIP5 climate simulation performed with coupled ECHAM6/MPIOM climate model (Taylor et al. 2012). The model reproduces reasonably well

the essential observed CGT features and associated precipitation over European region. Based on the above results, CGT emerges as one additional mode of mid-latitude atmospheric variability that can modulate significantly the European summer precipitation. However, the role of the other factors such as SNAO, the local land atmosphere coupling (e.g., Koster and Suarez 1995a, b; Schär et al. 1999; Seneviratne et al. 2006) also have serious impacts on European summer precipitation and therefore cannot be ignored.

In fact, previous studies showed that the regional precipitation variability can influence the upper level CGT (e.g., Ding and Wang 2005; Saeed et al. 2011b). The CGT-European summer precipitation linking mechanism is not fully clear from our analysis, and may involve processes in the North Atlantic sector as triggering factor of a series of feedbacks. In particular, we also found that warm SST anomalies in the western subtropical Atlantic Ocean along the southeastern US coast and the Gulf of Mexico could lead a positive CGT phase (Figs. 4a, 5). A plausible mechanism is: warm SST anomalies in the western subtropical Atlantic produce a deepening of the anomalous low pressure over the south-eastern US and adjacent areas. The intensification of the anomalous low pressure favors strong moisture convergence and associated precipitation over this region. The enhanced diabatic heating due to increased rainfall within the region (Hodson et al. 2010) may influence the upper level circulation that propagates eastward and modulates precipitation over the European region. This is also evident from the 200 hPa geopotential height composites associated with positive CGT and WEPI-CGT phases (Figs. 2a, 9a) which display strong upper level signals above this region (around 40°N and 100°W). A lead-lag relationship between SST over the western subtropical Atlantic and 200 hPa geopotential height over Atlantic is further supporting this hypothesis (Fig. 5).

Since the anomalous MSLP pattern over the Atlantic-European region is consistent with the upper level atmospheric circulation anomalies associated with the CGT, the SST anomalies in the subtropical Atlantic may also be a response of the circulation anomalies. A full feedback discussion is out of the scope of the paper and requires sensitivity model experiments to further explore this hypothesis. Since ECHAM6/MPIOM simulates reasonably well the observed CGT features, in a subsequent study we plan to further investigate the above hypothesis using the global model sensitivity experiments.

**Acknowledgments** This study is funded by the Belgian Science Policy (BELSPO) under the MACCBET Project. This research was further supported by the German Ministry of Education and Research (BMBF) under the MiKlip project. We thank the two anonymous reviewers for their constructive comment on this manuscript.

## References

- Blackburn M, Methven J, Roberts N (2008) Large scale context for the UK floods in summer 2007. *Weather* 63:280–288
- Bladé I, Liebmann B, Fortuny D, Jan van Oldenborgh G (2011) Observed and simulated impacts of the summer NAO in Europe: implications for projected drying in the Mediterranean region. *Clim Dyn*. doi:[10.1007/s00382-011-1195-x](https://doi.org/10.1007/s00382-011-1195-x)
- Branstator G (2002) Circumglobal teleconnections, the jet stream waveguide, and North Atlantic Oscillation. *J Clim* 15:1893–1910
- Christensen JH, Christensen OB (2003) Severe summertime flooding in Europe. *Nature* 421:805–806. doi:[10.1038/421805a](https://doi.org/10.1038/421805a)
- Colman A, Davey M (1999) Prediction of summer temperature, rainfall and pressure in Europe from preceding winter North Atlantic Ocean temperature. *Int J Climatol* 19:513–536
- Ding Q, Wang B (2005) Circumglobal teleconnection in northern hemisphere summer. *J Clim* 18:3482–3505
- Dirmeyer PA, Fennelly MJ, Marx L (2003) Low skill in dynamical prediction of boreal summer climate: grounds for looking beyond sea surface temperature. *J Clim* 16:995–1002
- Folland CK, Knight J, Linderholm HW, Federy D, Ineson S, Hurrell JW (2009) The summer North Atlantic oscillation: past, present and future. *J Clim* 22:1082–1103. doi:[10.1175/2008JCLI2459.1](https://doi.org/10.1175/2008JCLI2459.1)
- Giorgetta MA, Jungclaus J, Reick CH, Legutke S, Brovkin V, Crueger T, Esch M, Fieg K, Glushak K, Gayler V, Haak H, Hollweg HD, Ilyina T, Kinne S, Kornblueh L, Matei D, Mauritzen T, Mikolajewicz U, Mueller W, Notz D, Raddatz T, Rast S, Redler R, Roeckner E, Schmidt H, Schnur R, Segschneider J, Six KD, Stockhouse M, Wegner J, Widmann H, Wieners KH, Claussen M, Marotzke J, Stevens B (2012) Climate and carbon cycle changes from 1850 to 2100 in MPI-ESM simulations for the coupled model intercomparison project phase 5. *J Adv Model Earth Syst*. doi:[10.1002/jame.20038](https://doi.org/10.1002/jame.20038)
- Haylock MR, Hofstra N, Klein Tank AMG, Klok EJ, Jones PD, New M (2008) A European daily high-resolution gridded dataset of surface temperature and precipitation. *J Geophys Res* 113: D20119. doi:[10.1029/2008JD10201](https://doi.org/10.1029/2008JD10201)
- Hodson DLR, Sutton RT, Cassou C, Keenlyside N, Okumura Y, Zhou T (2010) Climate impacts of recent multidecadal changes in Atlantic Ocean sea surface temperature: a multimodel comparison. *Clim Dyn* 34(7–8):1041–1058. ISSN 0930-7575. doi:[10.1007/s00382-009-0571-2](https://doi.org/10.1007/s00382-009-0571-2)
- Hurrell JW (1995) Decadal trends in the North Atlantic oscillation: regional temperature and precipitation. *Science* 269:676–679. doi:[10.1126/science.269.5224.676](https://doi.org/10.1126/science.269.5224.676)
- Hurrell JW, Folland CK (2002) A change in the summer atmospheric circulation over the North Atlantic. *CLIVAR Exch* 7(3–4):52–54
- Jungclaus JH, Fischer N, Haak H, Lohmann K, Marotzke J, Matei D, Mikolajewicz U, Notz D, von Storch JS (2013) Characteristics of the ocean simulations in MPIOM, the ocean component of the MPI-earth system model. *J Adv Model Earth Syst*. doi:[10.1002/jame.20023](https://doi.org/10.1002/jame.20023)
- Kalnay E et al (1996) The NCEP/NCAR 40-year reanalysis project. *Bull Am Meteorol Soc* 77:437–470
- Kaplan A, Cane M, Kushnir Y, Clement A, Blumenthal M, Rajagopalan B (1998) Analyses of global sea surface temperature 1856–1991. *J Geophys Res* 103:567–589
- Koenigk T, Mikolajewicz U (2008) Seasonal to interannual climate predictability in mid and high northern latitudes in a global climate model. *Clim Dyn* 28:783–798. doi:[10.1007/s00382-008-0419-1](https://doi.org/10.1007/s00382-008-0419-1)
- Koster RD, Suarez MJ (1995) Relative contributions of land and ocean processes to precipitation variability. *J Geophys Res* 13775–13790. doi:[10.1029/95JD00176](https://doi.org/10.1029/95JD00176)
- Koster RD, Suarez MJ (1995b) Relative contributions of land and ocean processes to precipitation variability. *J Geophys Res* 100(D7):13775–13790. doi:[10.1029/95JD00176](https://doi.org/10.1029/95JD00176)
- Koster RD et al (2004) Regions of strong coupling between soil moisture and precipitation. *Science* 305:1138–1140. doi:[10.1126/science.1100217](https://doi.org/10.1126/science.1100217)
- Lenderink G, van Meijgaard E, Selten F (2009) Intense coastal rainfall in the Netherlands in response to high sea surface temperatures: analysis of the event of August 2006 from the perspective of a changing climate. *Clim Dyn* 32:19–33. doi:[10.1007/s00382-008-0366-x](https://doi.org/10.1007/s00382-008-0366-x)
- Marsh TJ, Hannaford J (2007) The summer 2007 floods in England and Wales—a hydrological appraisal. Centre for Ecology and Hydrology, Wallingford, p 32
- Meehl GA et al (2007) Global climate projections. In: Solomon S et al (eds) *Climate change 2007: the physical science basis*. Cambridge University Press, Cambridge, pp 747–845
- Müller WA, Baehr J, Haak H, Jungclaus JH, Kröger J, Matei D, Notz D, Pohlmann H, von Storch JS, Marotzke J (2012) Forecast skill of multi-year seasonal means in the decadal prediction system of the Max Planck Institute for Meteorology. *Geophys Res Lett* 39. doi:[10.1029/2012GL053326](https://doi.org/10.1029/2012GL053326)
- Ogi M, Yamazaki K, Tachibana Y (2005) The summer northern annular mode and abnormal summer weather in 2003. *Geophys Res Lett* 32:L04706. doi:[10.1029/2004GL021528](https://doi.org/10.1029/2004GL021528)
- Pal JS, Giorgi F, Bi X (2004) Consistency of recent European summer precipitation trends and extremes with future regional climate projections. *Geophys Res Lett* 31:L13202. doi:[10.1029/2004GL019836](https://doi.org/10.1029/2004GL019836)
- Qian B, Xu H, Corte RJ (2000) Spatial-temporal structures of quasi-periodic oscillations in precipitation over Europe. *Int J Climatol* 20:1583–1598
- Reynolds R, Smith T, Liu C, Chelton D, Casey K, Schlax M (2007) Daily high-resolution-blended analyses for sea surface temperature. *J Clim* 20:5473–5496
- Rodwell MJ, Drévillon M, Frankignoul C, Hurrell JW, Pohlmann H, Stendel M, Sutton RT (2004) North Atlantic forcing of climate and its uncertainty from a multi-model experiment. *Q J R Meteorol Soc* 130:2013–2032
- Saeed S, Müller WA, Hagemann S, Jacob D (2011a) Circumglobal wave train and summer monsoon over northwestern India and Pakistan; the explicit role of the surface heat low. *Clim Dyn* 37:1045–1060. doi:[10.1007/s00382-010-0888-x](https://doi.org/10.1007/s00382-010-0888-x)
- Saeed S, Müller WA, Hagemann S, Jacob D, Mujumdar M, Krishnan R (2011b) Precipitation variability over the South Asian monsoon heat low and associated teleconnections. *Geophys Res Lett* 38:L08702. doi:[10.1029/2011GL046984](https://doi.org/10.1029/2011GL046984)
- Schär C, Lüthi D, Beyerle U (1999) The soil-precipitation feedback: a process study with a regional climate model. *J Clim* 12:722–741
- Schär C, Lüthi D, Beyerle U (2004) The role of increasing temperature variability in European summer heatwaves. *Nature* 427:332–336. doi:[10.1038/nature02300](https://doi.org/10.1038/nature02300)
- Seneviratne SI, Lüthi D, Litschi M, Schär C (2006) Land atmosphere coupling and climate change in Europe. *Nature* 443:205–209. doi:[10.1038/nature05095](https://doi.org/10.1038/nature05095)
- Taylor KE, Stouffer RJ, Meehl GA (2012) An overview of CMIP5 and the experiment design. *Bull Amer Meteorol Soc* 93:485–498. doi:[10.1175/BAMS-D-11-00094.1](https://doi.org/10.1175/BAMS-D-11-00094.1)
- Trenberth KE (1999) Atmospheric moisture recycling: role of advection and local evaporation. *J Clim* 12:1368–1381
- Zanchettin D, Franks SW, Traverso P, Tomasino M (2008) On ENSO impacts on European wintertime rainfalls and their modulation by the NAO and the Pacific multidecadal variability described through the PDO index. *Int J Climatol* 28:995–1006. doi:[10.1002/joc.1601](https://doi.org/10.1002/joc.1601)